Desalination 513 (2021) 115129

Contents lists available at ScienceDirect

Desalination

journal homepage: www.elsevier.com/locate/desal

Modeling UF fouling and backwash in seawater RO feedwater treatment using neural networks with evolutionary algorithm and Bayesian binary classification

Yang Zhou [a], Bilal Khan [b,e], Han Gu [c], Panagiotis D. Christofides [d], Yoram Cohen [d,e,*]

[a] Laboratory of Smart Manufacturing in Energy Chemical Processes, East China University of Science and Technology, Ministry of Education, Shanghai 200237, China
[b] Department of Computer Science and Engineering, California State University, San Bernardino, CA, United States of America
[c] Orange County Water District, Research and Development Department, Fountain Valley, CA, United States of America
[d] Water Technology Research Center, Chemical and Biomolecular Engineering Department, Henry Samueli School of Engineering and Applied Science, University of California, Los Angeles, Los Angeles, CA 90095, United States of America
[e] Institute of the Environment and Sustainability, University of California, Los Angeles, Los Angeles, CA, United States of America

HIGHLIGHTS

- Machine learning (ML) developed to track UF seawater RO pretreatment performance.
- UF performance predicted by ensemble back propagation neural network (BPNN) model.
- UF ML model developed using 13 million data samples from a four year field study.
- Model accurately predicted UF performance during periods of varying water quality.

GRAPHICAL ABSTRACT

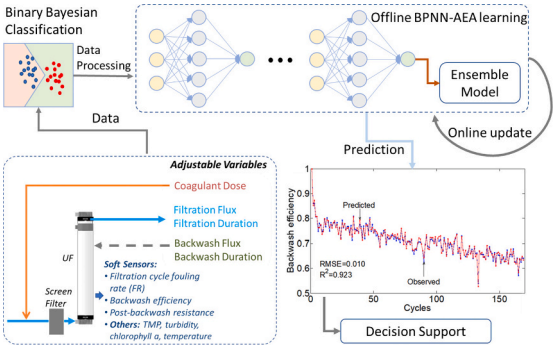

ARTICLE INFO

Keywords:
Ultrafiltration
Seawater RO feed pre-treatment
Backwash efficiency
Hydraulic membrane resistance
Back propagation neural network (BPNN)
Ensemble BPNN-AEA UF model

ABSTRACT

A machine learning approach to describing the dynamics of ultrafiltration performance in pretreatment of seawater reverse osmosis (RO) feedwater was explored via ensemble back propagation neural network (BPNN) model. The BPNN model was developed with Alopex evolutionary algorithm (AEA) optimization and AdaBoost strategy. The progression of ultrafiltration (UF) membrane resistance during both filtration and backwash, along with backwash efficiency were modeled via the ensemble BPNN-AEA approach relying on 422 days of operational data for an integrated SWRO UF-RO system. Model performance, for UF membrane resistance and backwash efficiency, evaluated over a wide range of operating conditions and coagulant dosing strategies, revealed excellent performance with a forecasting capability even for cases of temporally variable water quality. The performance level attained with the current machine learning modeling approach, which is particularly suited for handling the dynamics of UF operation, should prove useful for (a) determining UF performance

* Corresponding author at: Water Technology Research Center, Chemical and Biomolecular Engineering Department, Henry Samueli School of Engineering and Applied Science, University of California, Los Angeles, Los Angeles, CA 90095, United States of America.
E-mail addresses: profuc@gmail.com, yoram@ucla.edu (Y. Cohen).

https://doi.org/10.1016/j.desal.2021.115129
Received 5 March 2021; Received in revised form 27 April 2021; Accepted 27 April 2021

deviation from intended baseline performance, (b) forecasting expected UF performance due to anticipated changes in water quality, and (c) providing a basis for model-based control of UF operation.

1. Introduction

Dwindling fresh water supplies from traditional sources, coupled with more frequent drought conditions across the globe, intensify the need to develop alternative and sustainable potable water supplies [1,2]. In recent years, the deployment of reverse osmosis (RO) seawater and brackish water desalination and water reuse technologies have accelerated in various regions of the U.S. and around the globe as part of the movement to diversify the portfolio of available water resources. However, membrane fouling remains a major challenge for effective operation of both seawater and brackish water RO plants [3,4]. Effective RO feed water pretreatment is critical in order to reduce the propensity for RO membrane fouling by particulate/colloidal matter, biofoulants, and extracellular polymeric substances (EPS), the latter being particularly in littoral seawater [3,5–7]. RO membrane fouling degrades membrane performance (e.g., reduced permeability leading to increased applied pressure needed for a given target flux), thus increasing the frequency of required chemical cleaning, shortening membrane longevity and increasing operational costs [5,8–10].

In recent years, ultrafiltration (UF) has emerged as an attractive effective method for pre-treatment of RO feed water relative to other conventional options (e.g. sand filters, cartridge filters) [3,11–14]. UF membranes, having a pore size typically in the range of 0.01–0.1 μm, can remove particulates, colloids, microorganisms, and some dissolved organics matter (often with the aid of coagulant dosing), and accordingly produce high quality filtrate. UF operation for RO feed pretreatment is typically carried out in a dead-end filtration mode with periodic UF elements backwash to remove foulants buildup on the UF filters [11,15,16]. Both UF filtration and backwash effectiveness [17] can be improved through optimal coagulant dosing of the UF feed [7,8,18] and timed backwash frequency [16,17]. Coagulant dosing promotes floc formation (i.e., aggregation of fine particles and colloidal matter), thereby improving both UF and MF membrane filtration and hydraulic cleaning [19–22]. UF foulants that are not removed by backwash result in progressive irreversible foulant layer buildup, which at a certain threshold necessitate chemical cleaning-in-place (CIP) to restore UF membrane permeability [23,24]. To improve UF effectiveness and reduce overall cost associated with UF fouling [25,26] (e.g., due to chemical costs and possible loss of productivity), it is critical to optimize both UF filtration and backwash operations [16,27,28]. Accordingly, efforts have been devoted to elucidate the impact of various factors on UF fouling and backwash effectiveness that include, but are not limited to, feed water quality [17,20], filtration period length [15], backwash water composition [29], backwash flux [16,30], duration and frequency of backwash, UF feed coagulant dosing, CIP strategies and membrane properties [17,24,31,32].

Invariably, arriving at effective UF filtration and backwash strategies requires tracking the extent of UF fouling and assessment of backwash effectiveness. Conventional UF operations rely on tracking of UF fouling via the UF transmembrane pressure (TMP), UF filtration resistance or membrane permeability normalized with respect to their initial values in the filtration step post-CIP [7,16,20,33,34]. Admittedly, UF permeability loss due to fouling is a complex phenomenon governed by environmental factors (e.g., water source quality and temperature, and the stochastic nature of fouling phenomena). Clearly, establishing an effective UF process control strategy [35,36] would benefit from being able to describe the temporality of UF field performance along with quantification of fouling progression. At present, however, first principle mechanistic models of UF fouling fall short of being able to describe the dynamics of UF fouling and backwash effectiveness, particularly when continuous adjustments of coagulant, backwash flux and frequency may be required. In recent years, data-driven machine-learning (ML) UF operational models (for UF filtration and backwash) have been proposed based on artificial neural networks (ANNs) and support vector machine (SVM). ANNs models can handle non-linearities through complex interactions between neurons, but require large datasets and overfitting can be an issue when attempting to increase model predictive accuracy [37]. In contrast, SVM can handle the local minimum problem and is suitable for small sample size [38]. Irrespective of the utilized machine learning approach, sufficient data are necessary that spans a sufficient range of the operating parameters space to generate a state of the plant model capable of describing plant operation when subjected to variability of water quality and various operating conditions.

Confidence in developed ML models is predicated on the availability of real-time operational field data to describe temporal system patterns and utilize such information to arrive at suitable operational adjustments. Accordingly, the present work focused on investigating the complex relationships between various UF operational variables (include coagulant dosing) and UF fouling behavior as observed under field conditions for UF treatment of RO seawater feed. UF system behavior (i.e., impact of fouling on increased UF hydraulic resistance and backwash efficiency), was modeled via back propagation neural network (BPNN) models with Alopex evolutionary algorithm (AEA) (BPNN-AEA) model [37]. The data-driven models were developed based on extensive data generated from an integrated UF-RO seawater desalination field study. An ensemble learning approach (AdaBoost strategy) [39] utilizing a family of BPNN-AEA models was developed for a real system with over 13 million data samples collected over a period of four years. System performance, with respect to the evolution of post-backwash UF resistance and backwash efficiency, was evaluated under both normal and atypical conditions (e.g., storm event) using two variations of BPNN-AEA model. System operational data, which consisted of both typical and atypical operating conditions, enabled the development of robust and adaptive models whereby filtration and backwash modes were automatically recognized via binary Bayesian classification. The utility of the present approach was then evaluated with respect to predicting UF operating performance during temporally changing water quality.

2. Materials and methods

2.1. Integrated UF-RO seawater desalination system

Predictive BPNN-AEA models were developed based on operational data of UF seawater RO feed pretreatment in an integrated UF-RO desalination system (Fig. 1). Data were collected over the course of a four year study at the Naval Facilities Engineering and Expeditionary Warfare Center (NAVFAC-EXWC) at Port Hueneme, CA [40]. The integrated UF/RO system, described in detail elsewhere [15,41], had a permeate water production capacity of up to 66.8 m^3/day (17,640 GPD) utilizing three 8-in. RO elements (Dow Filmtec SW30HRLE-400, Dow Chemical Company, Midland, MI), and three inside-out polyethersulfone (PES) multi-bore hollow fiber (0.02 μm pore size) UF membrane modules (each having membrane surface area of 50 m^2; Dizzer 5000 +, Inge, Greifenberg, Germany) arranged in parallel. Feed water from open sea intake was pumped directly (offshore from the port) to a 7571 L (2000 gal) holding tank (< 3 h detention time) and then delivered to the RO pretreatment unit by a feed pump (XT100 SS, 3.73 kW, Price Pump, Sonoma, CA) controlled by a variable-frequency drive (VFD) (VLT AQUA Drive FC202, Danfoss, Denmark).

Feedwater to the UF modules was first filtered via an inline basket strainer (Hayward SB Simplex, Clemmons, NC), followed by a 200 μm self-cleaning microfilter (TAF-500, Amiad Corp., Mooresville, NC).

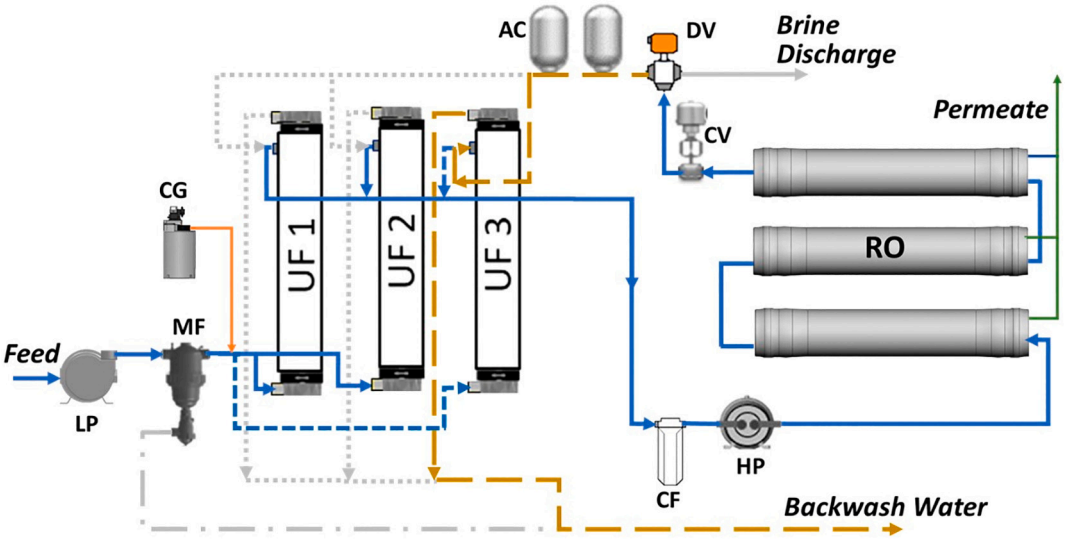

Fig. 1. Simplified schematic diagram of the UF-RO seawater desalination system showing an operational mode whereby UF modules 1 and 2 are infiltration mode while module 3 is undergoing backwash. (AC – hydraulic accumulator; CF – carbon filter; CV – retentate control valve; DV-flow splitter; HP – high pressure RO feed pump; LP – low pressure pump; MF – microfilter; UF – ultrafilters as three modules arranged in parallel; RO – RO elements in pressure vessels; CG – coagulant dosing unit). The various lines represent the following: thick solid lines - feed flow to and from filtering UF units and the RO elements feed-channels; Dashed-dot line – backwash stream from MF filter; Thin solid line – permeate streams; line with short dashes – feed flow to UF module 3 when either UF modules 1 or 2 are in backwash mode; Lines with wide dashes – RO concentrate backwash stream to UF module 1; Dotted lines – RO concentrate backwash to UF modules 1 and 2 when these undergo backwash.

Switching between filtration and backwash mode, and changing filtration/backwash directions (top or bottom) for the individual UF module banks was facilitated by electrically actuated 2 and 3 way ball valves [41]. Prior to delivery of the UF filtrate to the RO modules, it was passed through a cartridge filter (Ahlstrom Standard Disruptor) consisting of woven nano-alumina fibers (boehmite nanofibers) with a high adsorptive capacity for a wide range of dissolved organic matter (DOM). This filtration unit provided additional protection of the RO elements to capture both nanoparticles and potentially DOM that may have passed through the UF module.

UF Filtrate and backwash flowrates were monitored using magnetic flow meters (Signet 2551, George Fischer Signet, Inc. El Monte, CA) and hydraulic pressure was monitored via sensors (AST4000, American Sensor Technologies, Mt. Olive, NJ). Inline coagulant ($FeCl_3$) dosing of the UF feed at the UF pump inlet was accomplished using a metering pump (DDA 7.5–16, Grundfos, Bjerringbro, Denmark), to enhance the effectiveness of suspended matter removal and backwash efficiency [42]. A turbidity meter (Signet 4150, Georg Fischer Signet LLC, El Monte, CA), fluorometer sensor (Turner Designs, Cyclops-72,108, San Jose, CA), pH meter (Sensorex S8000CD, EM802/pH, Garden Grove, CA), and a temperature sensor (Signet 2350–3, George Fischer Signet LLC, El Monte, CA) were installed on the UF filtrate line. A summary of the relevant physical sensors and calculated process metrics used for model development are provided in Table 1.

2.2. Field study conditions

Seawater feed to the integrated UF-RO system was of variable quality over the study period. A summary of the range of intake water quality parameters is provided in Table 2. Feedwater turbidity, *Chlorophyll a* and total organic carbon levels varied over the ranges of 0.6–19 NTU, 12–300 μg/L and 0.7–1.3 mg/L, respectively. Seawater feed to the UF modules was not chlorinated and that UF backwash was accomplished without chemical additives. The RO unit was operated at 35% recovery without antiscalant dosing as scaling was not observed at this recovery level. A total of 178 short-term and 2 long-term UF filtration tests were carried out in three sequential phases. In the first phase, UF performance, with respect to progression of UF filtration fouling resistance and backwash effectiveness, was assessed for different inline coagulant ($FeCl_3$) dose levels for all 180 field tests (422 operational days). UF performance with coagulant dosing was evaluated for the range of 1.9–4.7 mg/L Fe^{3+} for fixed filtration periods, each of minimum of 64 filtration/backwash cycles. In the second phase, 178 tests were conducted to evaluate the impact of coagulant dose, backwash flux, duration, and frequency on UF performance.

Short UF tests were carried out over 15–60 min periods, each

Table 1
The description of UF-RO system sensors[a].

Parameter and description[a]	Parameter
UF Inflow Rate	$Q_{UF,feed}$
UF Element 1 (E1) Inflow rate	$Q_{UF,p1}$
UF Element 2 (E2) Inflow rate	$Q_{UF,p2}$
UF Element 3 (E3) Inflow rate	$Q_{UF,p3}$
UF Backwash Flow Rate	$Q_{UF,backwash}$
UF Filtrate pH	$pH_{UF,permeate}$
Microfilter (MF) Inlet Pressure	$P_{MF,feed}$
Microfilter (MF) Trans-filter Pressure	$\Delta P_{MF}=P_{MF,\ feed}-P_{MF,\ permeate}$
UF Inlet Filtration Pressure	$P_{UF,\ feed}$
UF Feed-Side Backwash Pressure	$P_{UF,\ feed,\ backwash}$
UF Filtrate Side Backwash Pressure	$P_{UF,\ backwash}$
UF Filtrate-Side Pressure	$P_{UF,permeate}$
UF Filtrate Turbidity	$Tu_{UF,permeate}$
UF Feedwater Turbidity (Post-MF)	$Tu_{UF,feed}$
UF Feed Pump RPM	V_{RPM}
UF Filtrate Temperature	$T_{UF,feed}$
Coagulant Dose)	d
N*FeedwaterChlorophyll a RFU (determined at pump house*[b]	$C_{UF,feed}$
Initial UF Resistance (Calculated Metric, Section 2.3)	$R_{UF,0}$
UF Filtration Duration	$t_{UF,filtration}$
UF Backwash Flux	$J_{UF,\ backwash}$
UF Backwash Duration	$t_{UF,backwash}$

[a] Online sensor data was acquired at a frequency of 1 Hz; Unless otherwise indicated all variables relate to the UF unit; E1, E2 and E3 denote the first, second and third UF elements, respectively.

[b] Raw seawater pumped from open intake. Note: Filtration and backwash modes were categorical parameters designating the corresponding operational periods.

Table 2
Seawater quality datasets for the study period at the study field site.

No. of Datasets	Dataset Type	No. of operating days (No. Cycles)	Turbidity (NTU)	Chlorophyll (RFU, μg/L)	Coagulant dose[c] (mg/L Fe^{3+})	pH	Temperature (°C)
180	Total	422 (18014)	[0.6, 19.0]	[12, 300]	[1.9, 4.7]	[7.5, 8.2]	[11.2, 25.6]
150	Training[a]	324 (14287)	[0.6, 17.7]	[12, 260]	[1.9, 4.7]	[7.5, 8.0]	[11.2, 25.6]
30	Test[b] (total)	98 (3727)	[0.9, 19.0]	[32, 300]	[1.9, 4.4]	[7.5, 8.2]	[12.5, 24.9]
1[d]	Test (#TE1)	13 (689)	[1.3, 2.3]	[46, 98]	2.7	[7.8, 8.0]	[19.7, 24.0]
1[e]	Test (#TE10)	3 (142)	[3.4, 5.1]	[75, 89]	2.7	[7.9, 8.2]	[12.7, 17.0]
1[f]	Test (#TE15)	3 (130)	[1.5, 3.2]	[61, 124]	[2.6, 3]	[7.7, 7.9]	[17.3, 21.9]
1[g]	Test (#TE22)	4 (170)	[0.6, 4.4]	[58, 244]	2.7	[7.7, 8.1]	[14.3, 16.4]
1[h]	Test (#TE23, Storm)	8 (520)	[1.5, 19]	[43, 142]	[3.6, 4.4]	[7.6, 8.1]	[14.8, 17.1]

[a] 150 training datasets of which 47 were for UF operation at variable coagulant dose (mg/L as Fe^{3+}) for the ranges: [1.9, 3], [2.6, 3] and [3.6, 4.7].
[b] Thirty test datasets of which 15 sets were with variable coagulant dose in the range of 1.9–4.4 mg/L Fe^{3+}.
[c] Coagulant dose range for the indicated dataset types or dataset number.
[d] Dataset #TE1–13 day operational period.
[e] Dataset #TE10–3 days of operation with variable filtration cycle duration.
[f] Dataset #TE15 - UF operation at a progressively increasing and then decreasing coagulant dose.
[g] Dataset #TE22 - UF operation during the widest variability of feedwater *Chlorophyll a* and turbidity.
[h] Dataset #TE23 - acquired during a storm event.

consisting of at least 12 filtration/backwash cycles. The third phase focused on two longer term (>240 h) tests in which various fouling indicators were quantified to characterize UF filtration and backwash performance during periods of temporal variability of feedwater quality. At the end of each test, the UF modules were backwashed with the RO concentrate for two minutes at a flux of 162 L/m^2h (approximately 3.6-fold the filtration flux). Chemical cleaning in place was carried out approximately every two months following a manufacturer protocol using an alkaline detergent and surfactant solutions.

UF filtrate turbidity, *chlorophyll a* and TOC levels were <0.03 NTU, <0.7 μg/L, and <0.5 mg/L, respectively. Throughout the study duration, the RO elements were well protected by UF pretreatment of the RO feed as reported in previous studies with the integrated UF-RO system at the same location [15,17,41]. The permeability and salt rejection of the RO elements remained stable at $1.85 \pm 0.137 \times 10^{-12}$ m/Pa·s and ~ 99.5% over the course of the four-year study. It is also noted that RO Permeate salinity and TOC were consistent at levels of 148 ± 13 mg/L TDS and < 0.5 mg/L, respectively.

2.3. Online UF fouling and performance indicators

UF pretreatment of RO feed water was carried out at constant filtration flux in a "dead-end" mode. Each UF cycle comprised of a filtration period and a subsequent backwash period as illustrated in Fig. 2. The critical UF performance indicators utilized in the study were the time-dependent UF membrane resistance during filtration, post-backwash UF resistance and its evolution, as well as backwash efficiency [43]. These metrics were based on real-time monitoring of UF process parameters which included filtrate and backwash durations, filtration backwash fluxes, corresponding feed-side and filtrate-side pressures, in addition to coagulant dose, feedwater turbidity, *chlorophyll a* and feed temperature.

UF filtration resistance was determined given the measured filtration flux, J_F (m/s), and transmembrane pressure, ΔP (kPa), where the filtration flux was expressed as $J_F = \Delta P/\mu R_t$, in which μ is the feed water viscosity (Pa·s), and the overall (or total) membrane hydraulic resistance is denoted by R_t [42]. The typical resistance-in-series model [44]

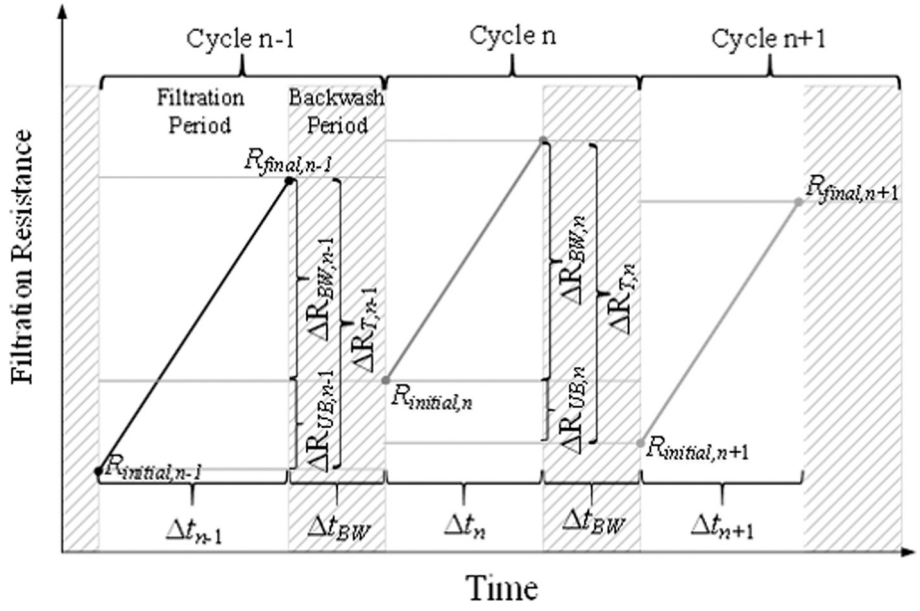

Fig. 2. Illustration of the operation (filtration/backwash) cycles. $R_{initial,n}$ and $R_{final,n}$ are the initial and final UF membrane resistances, respectively ($\Delta R_{T,n} = R_{final,n} - R_{initial,n}$) for cycle n filtration duration of Δt_n, and $\Delta R_{UB,n}$ is the cycle n unbackwashed portion of the membrane fouling resistance buildup from cycle n-1. ($R_{initial,n}$ also represents the post-backwash resistance associated with cycle n-1 and $\Delta R_{BW,n} = \Delta R_{T,n} + \Delta R_{UB,n}$). (Adapted from [43]).

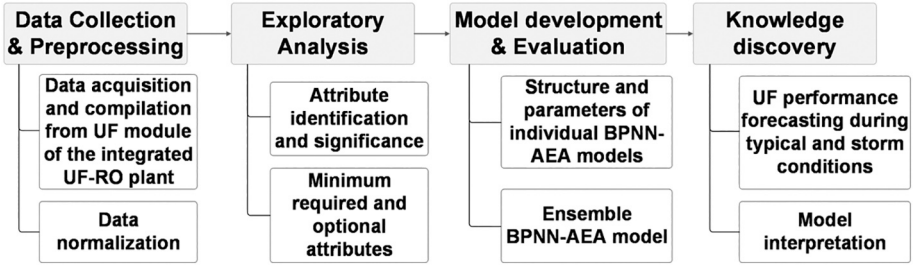

Fig. 3. Workflow for UF filtration and backwash efficiency assessment and BPNN-AEA model development.

was used to describe the total resistance expressed as R_t=R_m+R_{cake}+R_{irr}, in which R_m, R_{cake}, and R_{irr} represent the hydraulic resistance of the clean membrane, and the added foulant cake and irreversible fouling resistances, respectively. The cake layer that builds on the membrane surface which can be removed by backwash is regarded as the reversible fouling resistance. The irreversible resistance is attributed to the foulant not removed by backwash. For a given filtration cycle *n*, the initial UF resistance ($R_{initial,n}$) (i.e., post-backwash resistance for cycle *n-1*), the final UF filtration resistance ($R_{final,n}$), and filtration duration (Δt_n) were computed based on the measured UF transmembrane pressure and filtration flux.

For a given cycle, *n*, the increase in UF fouling resistance, $\Delta R_{T,n}$ (i.e., $R_{final,n}$ - $R_{initial,n\text{-}1}$) was expressed as $\Delta R_{t,n}$=$\Delta R_{UB,n}$+$\Delta R_{BW,n}$, in which resistance removed in the previous backwash period is given by $\Delta R_{BW,n}$ = $R_{final,n}$ - $R_{initial,n}$, and the unbackwashed fouling resistance is $\Delta R_{UB,n}$ = $R_{initial,n}$ - $R_{initial,n\text{-}1}$. With progressive filtration/backwash cycles the change in $\Delta R_{UB,n}$ is indicative of the foulant removal efficacy by UF backwash. In principle, ΔR_{UB} can be negative (i.e., $\Delta R_{UB} \gg R_{irr}$) when foulant removal, in a given cycle, is greater in comparison with the previous cycle (e.g., due to changing environmental conditions and improved water quality). The above behavior can occur when foulant not removed from the UF elements in a given backwash cycle is partially or completely removed in subsequent backwash cycles. The progression of post-backwash (PB) UF resistance for each cycle, i.e., $R_{PB,\ n}$ - $R_{initial,\ n+1}$, and the ability to reduce the rate of *PB* resistance (R_{PB}) increase are governed by the ability to reduce the cycle-to-cycle unbackwashed membrane resistance ($\Delta R_{UB,\ n}$) increase. The progressive post-backwash resistance increase with progressive filtration/backwash cycles is given by:

$$R_{PB} = \sum_{n=0}^{N}\left(R_{PB,n-1} - R_{initial,n-1}\right) = \sum_{n=0}^{N}\Delta R_{UB,n} = R_{initial,N} - R_{initial,0} \tag{6}$$

where R_{PB}, which is indicative of the overall state of UF membrane fouling, is the summation of the cycle-to-cycle UF unbackwashed resistance change, and where $R_{initial,N}$ and $R_{initial,0}$ are the final post-backwash and initial UF membrane filtration resistances, respectively. Finally, the efficiency of UF backwash ($BW_{eff,n}$) for a given cycle [16] can thus be conveniently expressed as,

$$BW_{eff,n}(\%) = \frac{\Delta R_{BW,n}}{\Delta R_{T,n}} \cdot 100 = \left(1 - \frac{\Delta R_{UB,n}}{FR_n \cdot \Delta t_n}\right) \cdot 100 \tag{5}$$

in which $BW_{eff,n}$(%) represents the percentage of removed fouling resistance, and FR_n is the fouling rate for the given filtration cycle *n,* i.e., FR_n=$\Delta R_{T,n}$/Δt_n. The above fouling metrics and backwash efficiency were determined based on the compiled UF performance datasets (Table 2, Table S1, Section S1 Supplementary Material) and then utilized for model building as described in Section 2.2.

2.4. Workflow

UF data-driven Back Propagation Neural Networks, with Alopex-based evolutionary algorithm (BPNN-AEA), were developed as ensemble BPNN-AEA models to describe UF resistance (during filtration and backwash) and backwash efficiency, respectively. The above model development followed the workflow shown in Fig. 3. Briefly, after data collection and preprocessing, exploratory data analysis was carried out to remove attributes redundancy and then evaluate attribute significance based on model performance, thereby establishing the reasonably needed (and optional) set of model attributes (Section 2.6). Subsequently, the identified significant attributes were used to establish an ensemble BPNN-AEA model that provides predictions based on a weighted aggregation of ourcomes from the individual BPNN-AEA models. Finally, the ensemble BPNN-AEA model was tested using both normal and storm data demonstrating the utility of the modeling approach for forecasting UF operational performance. Model training and test datasets comprised of 150 and 30 UF operational tests, respectively, whereby the overall dataset consisted of a total of 13.4 million raw data samples, each with the 22 quantitative attributes listed in Table 1.

2.5. Data collection and preprocessing

UF operational performance was determined based on measurements from multiple sensors (Table 1). The compiled dataset were interrogated with respect to attribute correlations to enable pruning (i.e., model tuning) for final BPNN-AEA model development. The overall dataset was compiled from 53 thousand UF operational cycles, acquired from a four-year study (2012–2015), and comprised of 180 distinct field tests of durations ranging from hours to 45 days. Each UF cycle consisted of a filtration period followed by a backwash period. A summary of the field tests with the relevant attribute definitions and their ranges is provided in Table 2. The compiled data, comprising of 180 datasets, were split into two sets of 150 and 30 datasets for BPNN-AEA model training and testing, respectively. Model training with binary Bayesian classification was then carried out to enable the BPNN-AEA model to switch between the two distinct UF operational filtration and backwash modes.

The BPNN-AEA models for UF resistance and backwash efficiency were developed based on the attributes of greatest significance (Section 2.6). Model attributes were normalized in the range of [0,1] as $(x - x_{\min})/(x_{max} - x_{\min})$ for $n = 1,2, \ldots,N$ where N is the total number of data samples, and x_{min} and $x_{\max}$ are the minimum and maximum reported values in a dataset, respectively. UF resistance and backwash efficiency data revealed temporal irregularity (i.e., the mean values were non-stationary for the time-series data) and followed non-stationary stochastic patterns with non-uniform statistical measures (i.e., increasing or decreasing mean value) [45]. Accordingly, for BPNN-AEA model

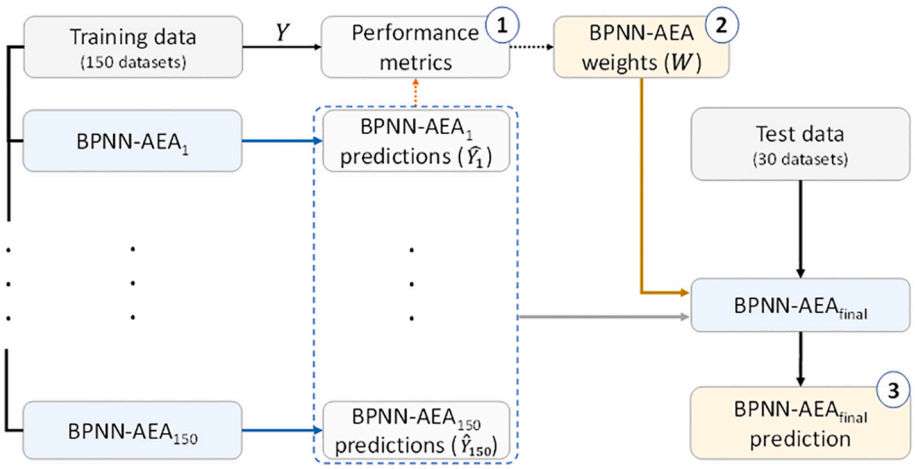

Fig. 4. Flowchart of the ensemble BPNN-AEA method. Model predictions from each BPNN-AEA model were used to calculate individual BPNN-AEA model performance metrics (i.e., R^2 and RMSE, i.e., box 1). These performance metrics were utilized to derive a weight function assigning a weight to each of the BPNN-AEA models (i.e., box 2) used for the ensemble model weighted average predictions (box 3), for the target scenario, based on the predictions of the individual 150 BPNN-AEA models ($Y_{ensemble}$).

development, non-stationarity was removed via a second order differencing [46].

2.6. Data exploration and attribute selection

In order to address the tradeoff between model complexity and performance, the importance of each individual attribute was initially assessed using BPNN-AEA models developed for all 22 attributes (Table 1). These attributes were selected as the basic process variables most likely toimpact UF filtration and backwash [43]. The feed forward feature selection (FFFS) [47] and minimal redundancy maximal relevance (mRMR) were used to initially identify and then rank the attributes assessed individually with respect to model performance (Fig. S1, Section S2, Supplementary Material). Subsequently, the assessment of attribute significance was carried out iteratively, whereby in each iteration an attribute was sequentially added to the model. An attribute was considered significant and retained as part of the model attribute set when model improvement due to said attribute increased by $R^2 > 0.01$. This process continued until no discernible increase in R^2 was observed (i.e., incremental increase in R^2 was <0.01; Section 3.1, Fig. 5).

2.7. AdaBoost BPNN model with AEA optimization algorithm

Machine learning models for ultrafiltration (UF) resistance and backwash efficiency (Sections 3.2, 3.3) were developed based on back propagation neural network (BPNN) models [37] following the workflow described in Fig. 3. Given the high level of data diversity (Table 2), independent BPNN models were developed, and trained utilizing 150 datasets (Section 2.5) based on the adaptive boosting (AdaBoost) ensemble method [39]. It is noted that the BPNN-AEA models were each applicable for the different ranges of temporally varying water quality and operating conditions. The ensemble model was then developed whereby predictions from the family of the individual BPNN models were weighted to arrive at a single final ensemble model prediction for the target input attributes [47,48]. Detailed description of the ensemble learning (AdaBoost) approach can be found elsewhere [39]. Model attributes (i.e., input variables) were selected via a forward feature selection approach [47]. The BPNN models were tuned via optimization to minimize the loss function (i.e., the squared difference between the observed and predicted outcomes, i.e., UF resistance and backwash efficiency). At each iteration the loss function for each model was minimized via the backpropagation algorithm until the given model converged (i.e., the convergence threshold of 10^{-5} in term of the normalized model output) [37,49]. In the above approach, model weights were fine-tuned at every training step, thereby increasing model generalizability. Tuning of weight updates per epoch was enhanced using the Alopex-based evolutionary algorithm (AEA) [50,51].

In the present study, the BPNN-AEA model structure was with 7 input nodes, one layer of 15 hidden nodes and 1 output node. Each BPNN-AEA model comprised of a filtration and a backwash mode. Binary Bayesian classification was introduced to adaptively identify the filtration and backwash modes and overcome data non-uniformity and high variance

Table 3
Identified most significant and other relevant model attributes.

Minimum set of required attributes	BPNN-AEA UF Model Attributes (F- filtration, B-backwash)		Attribute impact
	All	Storm	
ΔP_{MF} (MF Trans-filter pressure)	F	F	Increases with rising feedwater fouling propensity
$\Delta P_{UF\text{-}Filtrate}$ (transmembrane pressure during filtration)	F	F	Higher transmembrane pressure results in higher permeate flux and higher rate of fouling
$\Delta P_{UF\text{-}Backwash}$ (transmembrane pressure during backwash)	B	B	Higher backwash permeate pressure, for a target backwash flux, is indicative of greater foulant buildup from the filtration period
Initial UF resistance	F, B	B	The initial resistance at the beginning of each filtration period
Coagulant dose	F, B	F, B	Coagulant dose increases UF filtration and backwash efficiency up to a critical level. [43]
UF feed water turbidity	F, B	F, B	Required UF feed pressure increases with feedwater turbidity and can lead to decreased backwash efficiency
Filtrate temperature	F, B	F, B	Foulant adherence to the UF membrane surface may vary with temperature
Backwash duration	B	B	Longer backwash duration will improve backwash efficiency but may lead to longer filtration period to attain the target filtrate productivity
Optional attributes:			
Filtrate pH	F	F	Membrane surface fouling may be affected by pH
Chlorophyll a RFU[a]	F, B	F, B	Greater UF fouling and possibly lower backwash efficiency may be associated with increasing *Chlorophyll a* RFU
Backwash flux	B		Backwash efficiency is expected to increase at higher backwash flux

[a] *Chlorophyll a* RFU variability was significant primarily during the storm event (Table 2).

for robust prediction. The sets of model parameters of each BPNN-AEA model were aggregated to form a generalized BPNN-AEA ensemble model (Fig. 4) to describe both the filtration and backwash operational modes for each UF operation cycle. The ensemble model was validated using a set of 30 test datasets (Table 2).

Model performance metrics (i.e., R^2 and *RMSE* - box 1 in Fig. 4) were calculated using each BPNN-AEA model predictions $\{\widehat{Y}_1, \widehat{Y}_2, \ldots, \widehat{Y}_{150}$ – blue dashed box in the middle column of Fig. 4} which were then used to derive a weight function $W=\{\omega_1,\ldots,\omega_{150}\}$ (box 2 in Fig. 4), for each model k {k = 1,2, …150), as given by $\omega_k = \pi_k / \sum_{j=1}^{150}\pi_j$ in which $\pi_k = 1/(R^2_{avg}/R^2_k + RMSE_k/RMSE_{avg})$. Given the above, model outcome prediction ($Y_{ensemble}$) for an operational scenario (i.e., based on the model attributes) was based on a weighted average of the individual BPNN-AEA models [37,39], as per the AdaBoost approach, given by $Y_{ensemble} = \sum_{k=1}^{150}\omega_k * \widehat{Y_k}$. The above approach enabled predictions that are specific to the operating conditions range over the entire training datasets, as well as the 30 test datasets that included a storm event.

Performance of BPNN-AEA models was quantified by the root-mean-squared error (RMSE) and R-squared. RMSE was determined from $\text{RMSE} = \sqrt{\sum_{i=1}^{N}\left(y_i - \widehat{y}_i\right)\Big/N}$. R-squared, which was calculated as $R^2 = 1 - \sum_{i=1}^{N}\left(y_i - \widehat{y}_i\right)^2 / \sum_{i=1}^{N}\left(y_i - \bar{y}\right)^2$, represents the variance proportion in the dependent variable (UF resistance or backwash efficiency) that is predictable based on the independent variables, where N is the number of test samples, and $\bar{y}$ and $\widehat{y_i}$ are the average and predicted (model estimated) values, respectively.

The deployed ensemble learning approach required ~10 min for training the final ensemble BPNN-AEA model, while the validation of one set of input parameters (i.e., one sample) was essentially instantaneous on a PC with i7 Processor and 32 GB RAM. In addition, updating of a new ensemble BPNN-AEA model with a new dataset of size in the range

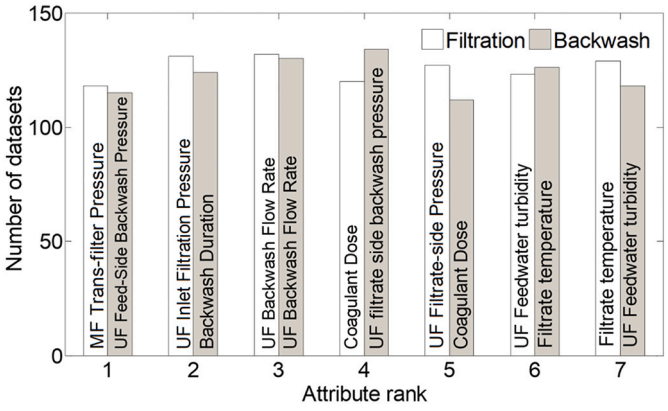

Fig. 6. The number of datasets in which the listed top seven attributes were ranked as indicated.

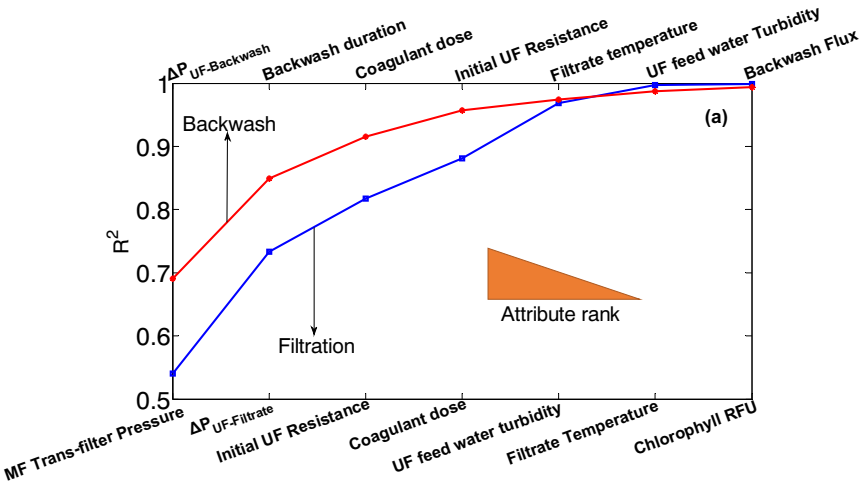

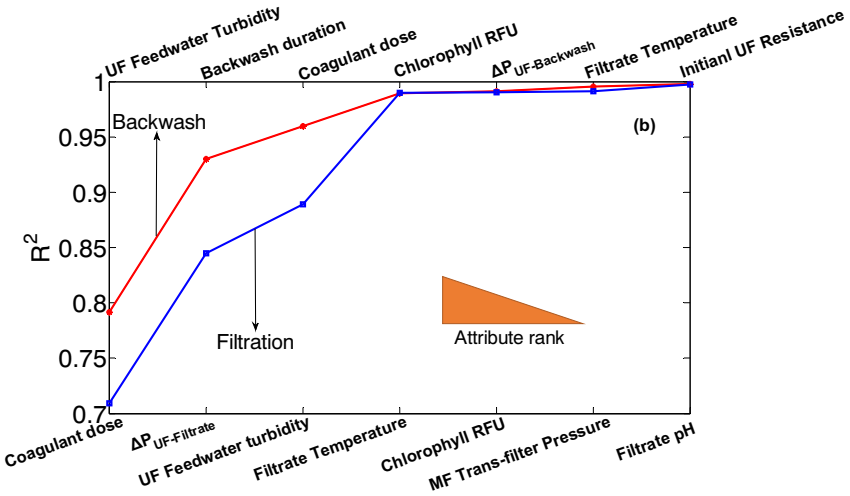

Fig. 5. BPNN-AEA model prediction accuracy for the most significant attributes identified via FFFS approach based on the (a) 150 training datasets (Section 2.2, Table 2), and (b) a storm event (dataset #TE23, Table 2). The indicated attributes (Table 1) were incrementally added to those previously selected by FFFS for each BPNN model and the R^2 values of each BPNN model for the included attribute were then averaged (Datasets 1–150)). The order of attribute selection by the FFFS based on the highest R^2 also infers its importance to the correlation.

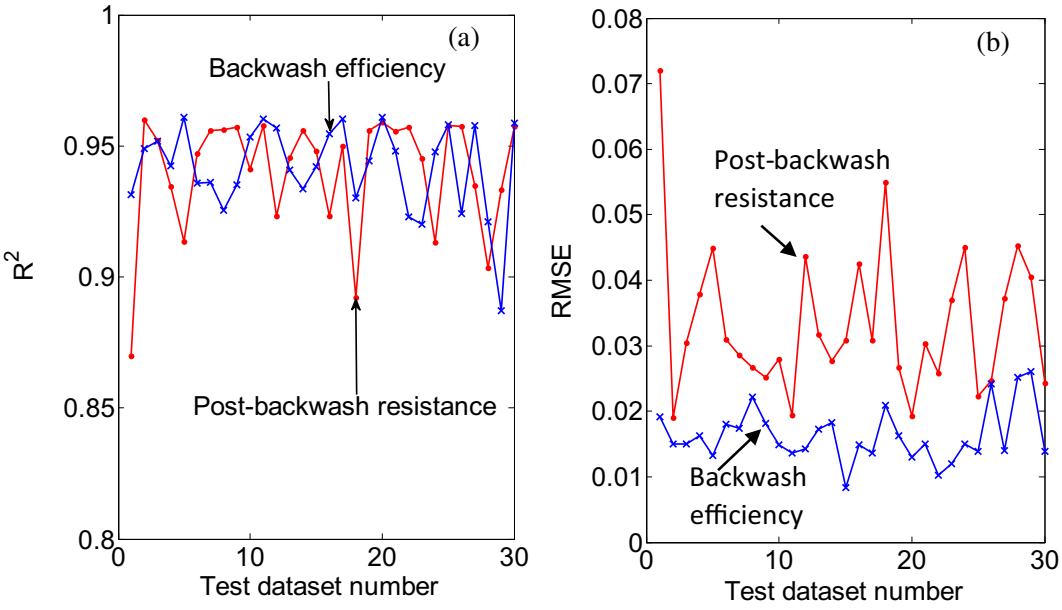

Fig. 7. Performance of the BPNN-AEA models, using the minimum attribute set (Table 3), for the 30 test datasets in terms of (a) R^2, and (b) RMSE for post-backwash UF resistance and backwash efficiency using the minimum attribute set (Table 3). The ranges of R^2 and RMSE for are provided in Table 4.

of the current datasets required ~20 seconds to calculate the new BPNN-AEA model parameters and associated model scores for the independent models in the ensemble.

3. Results and discussion

3.1. Exploration of attribute relevance to modeling of post-backwash UF-resistance and backwash efficiency

In order to assess the most relevant set of attributes for the BPNN-AEA models, the significance of each attribute in the initial attribute pool (Table 2) was evaluated with the attributes ranked based on the FFFS approach (Section 2.6). The average R^2 values for the most significant attributes (Table 3) were determined, based on 150 BPNN-AEA models developed following the workflow presented in Fig. 3. The R^2 values are presented in Fig. 5, in the order of their decreasing importance. Ranking of the identified significant attributes and a summary of the number of datasets that supported their ranking are provided in Fig. 6. In all cases, the ranking was supported by more than 100 of the 150 datasets used for assessing attribute significance. The same set of top 10 attributes were also identified via a mRMR coefficient analysis (Section S2, Supplementary Material) of the data using the 22 model attributes (Table 1). Performance of the above individual models with the top ten attributes, for their respective training datasets, was with R^2 ~ 0.78–0.92 and RMSE ~0.015–0.132, and R^2 ~ 0.76–0.91, RMSE ~0.01–0.08 for the post-backwash UF resistance and backwash efficiency models, respectively.

Predictive performance of the ensemble BPNN-AEA model (Section 2.7, Fig. 4), based on the 150 training datasets, was evaluated with respect to predictive performance for each of the 30 test datasets (Fig. 7). Predictive performance of the ensemble models for the post-backwash UF resistance and backwash efficiency models, based on the 30 test datasets, with the minimum attributes set (Table 3), was with R^2 ~ 0.87–0.96 and RMSE ~0.019–0.072, and R^2 ~ 0.89–0.96, RMSE ~0.013–0.0260, respectively. The distributions of R^2 and RMSE for predictions of the post-backwash resistance and backwash efficiency, averaged over the 30 test datasets, were R^2 ~ 0.945, *RMSE* ~ 0.0325 and R^2 ~ 0.922, *RMSE* ~ 0.0154, respectively. Addition of the optional attributes for modeling post-backwash resistance and backwash efficiency (Table 3), slightly improved the corresponding model predictions to R^2 ~ 0.96, *RMSE* ~ 0.0277 and R^2 ~ 0.94, *RMSE* ~ 0.0137, respectively. Overall, it is apparent that BPNN-AEA model predictions were quite reasonable for filtration (i.e., post-backwash resistance) and backwash efficiency, even with merely the top 5 and 6 attributes, respectively (Fig. 5), over a wide range of raw water quality (Table 2) and coagulant dose. It is noted that during periods of significant water quality fluctuations, experienced during a four-day storm event (Table 2), inclusion of the attributes *Chlorophyll a* RFU and Filtrate pH slightly improved model performance. The post-backwash resistance model (for the filtration) R^2 increased (by 0.005) to 0.945, and *RMSE* decreased (by 0.005) to 0.0236, while for backwash efficiency predictions R^2 increased to 0.92 (i.e., improved by 0.02) and *RMSE* decreased (by 0.006) to 0.016.

Table 4
Ensemble BPNN-AEA model performance for hydraulic UF resistance, backwash efficiency and post-backwash resistance predictions based on the complete attribute set for the 30 test datasets[a].

Prediction Performance Metrics	Typical Operation[b]		Storm Event[c]	
	Hydraulic Resistance			
	Filtration	Backwash	Filtration	Backwash
R^2	0.923–0.98 (Avg 0.962)	0.90–0.968 (Avg 0.948)	0.945	0.934
RMSE	0.012–0.051 (Avg 0.0273)	0.021–0.059 (Avg 0.0317)	0.039	0.053

	Backwash Efficiency	$<R_{PB}>/<R_{PB}>_0$	Backwash Efficiency	$<R_{PB}>/<R_{PB}>_0$
R^2	0.917–0.972 (Avg 0.942)	0.91–0.967 (Avg 0.947	0.92	0.92
RMSE	0.008–0.016 (Avg 0.0135)	0.010–0.02 (Avg 0.013)	0.012	0.016

[a] Attribute set is provided in Table 2.
[b] based on the collection of the 30 test datasets (Table 2).
[c] Dataset #TE23 (4-day storm event).

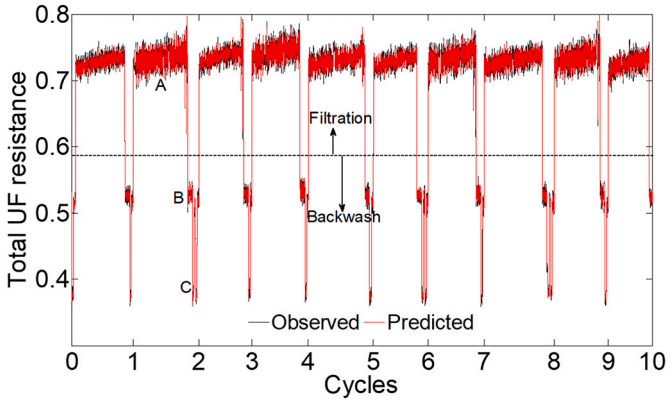

Fig. 8. Example of BPNN-AEA model (with binary Bayesian classification) prediction of UF resistance (for filtration and backwash operational modes) for the first ten of the 142 cycles of test dataset #TE10 dataset corresponding to Fig. 9.

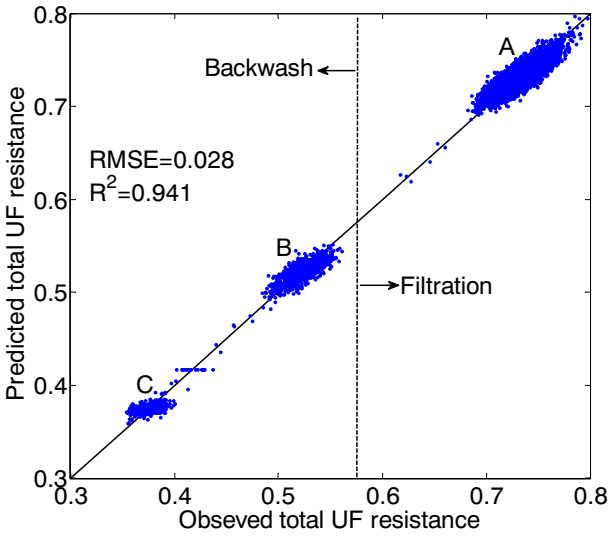

Fig. 9. BPNN-AEA model (with binary Bayesian classification) predictions of UF resistance (for both the filtration and backwash operational modes) under typical operating conditions over a period of 3 days comprising of 142 UF filtration cycles (Dataset #TE10). The vertical dashed line represents the separation between the UF filtration (right) and backwash processes. (Note: turbidity, and *Chlorophyll a* ranges were 3.4–5.1 NTU and 61–124 μg/L respectively, with UF operation at a constant coagulant dose of 2.7 mg/L Fe^{3+}).

3.2. BPNN-AEA model for UF resistance and backwash efficiency

The range of UF hydraulic resistance prediction accuracy of the ensemble model, for the filtration and backwash operational periods, for the 30 test datasets, is given in Table 4. The ensemble models R^2 for the filtration and backwash hydraulic resistances were in the range of 0.92–0.98 and 0.9–0.97, respectively, with RMSE below 0.051 for all cases. Backwash efficiency and post-backwash UF resistance predictions for the test datasets were of comparable high levels with RMSE below 0.016 and 0.02, respectively (Section 3.3, Table 4). It is interesting to note that model predictions of UF performance for the storm event dataset (Table 2), during which the range of feed water turbidity and *Chlorophyll a* varied significantly during a 4-day period (Table 2), were equally good with R^2 of 0.945 and 0.934 for the hydraulic resistance during UF filtration and backwash, respectively, with the corresponding RMSE for the above periods being 0.023 and 0.033. Model performance for backwash efficiency and for post-backwash UF resistance during the storm event were also of reasonable accuracy with R^2 of 0.92 and 0.94, respectively and corresponding RMSE of 0.012 and 0.028.

An illustration of the ensemble BPNN-AEA model (based on AdaBoost) prediction for UF post-backwash resistance that encompasses both the filtration and backwash periods is shown in Fig. 8 (dataset *#TE1*) demonstrating prediction accuracy of $R^2 \approx 0.941$ with $RMSE \approx 0.028$ (Fig. 9). Predictions for the UF filtration mode (group A above the horizontal dashed line in Fig. 8 and to the right of the dashed vertical line in Fig. 9) were with $R^2 \approx 0.95$ with $RMSE \approx 0.022$. There are noticeable groupings in Fig. 9, left of the vertical dashed line, which are associated with the two backwash modes (B and C; below the horizontal dashed line in Fig. 8) that exist in the present UF system (Section 2.1). The middle grouping (B) is for post-backwash UF filtration resistance after concentrate backwash at a constant permeate flux, while the lowest grouping (C) is for post-backwash resistance attained after additional pulse backwash [43]. The above groupings that are associated with the different operational modes are evident in the illustration of Fig. 8, demonstrating a rise in UF resistance during filtration (region above the middle horizontal line). In the backwash region (below the horizontal dashed line) UF resistance decreases during constant UF backwash (B) and rises to a significantly greater degree when pulse backwash is active (C). The accuracy of predictions as illustrated in Figs. 8 and 9 confirms the adequacy of the identified minimum set of process attributes for tracking membrane filtration resistance for both the UF filtration and backwash periods.

3.3. Ensemble BPNN-AEA model performance during conditions of fixed and variable coagulant dosing strategy

The majority of the training datasets (103 groups) were for a fixed coagulant dosing strategy (range of 2.7–3.5 mg/L Fe^{3+}), while 15 of the test datasets were for UF operation under variable coagulant dosing in the range of 1.9–4.4 mg/L Fe^{3+}. Model performance, with the complete attribute set (Table 3) for the latter 15 test datasets was with $R^2 \sim$ 0.94–0.98 and RMSE ~0.012–0.047 for UF resistance and $R^2 \sim$ 0.937–0.972, RMSE ~0.008–0.017 for backwash efficiency. Operation with suboptimal coagulant dose [43] would lead to rapid decline in backwash efficiency and as a consequence progressive increase of UF post-backwash resistance. This scenario is illustrated in Fig. 10a and Fig. S2 (Section S3, Supplementary Material) for dataset #TE22 for operation 170 cycles (over 4 days) at a constant coagulant dose of 2.7 mg/L Fe^{3+}. During the above operational period *Chlorophyll a* and turbidity were high and in the range of 58–244 mg/L and 0.6–4.4 NTU, respectively (Fig. 10c). It is interesting to note that the backwash efficiency typically declined when spikes of worsening water quality were encountered as can be seen, for example, for UF cycles 86 and 132. Overall, the BPNN-AEA model for backwash efficiency (using the complete attribute set) demonstrated good performance with R^2 of 0.923 and RMSE of 0.01 (Fig. 10b) tracking the progressive decrease in declining backwash efficiency. The above behavior was likely the result of ferric chloride coagulant dose which was well below the reported critical threshold dose (i.e., above which further backwash efficiency enhancement was not observed) of ~4.16 mg/L Fe^{3+} for the present UF system treatment of seawater [43]. Model predictions of post-backwash resistance for the filtration and backwash periods were also at a reasonable level of $R^2 \sim 0.932$ and RMSE~0.045.

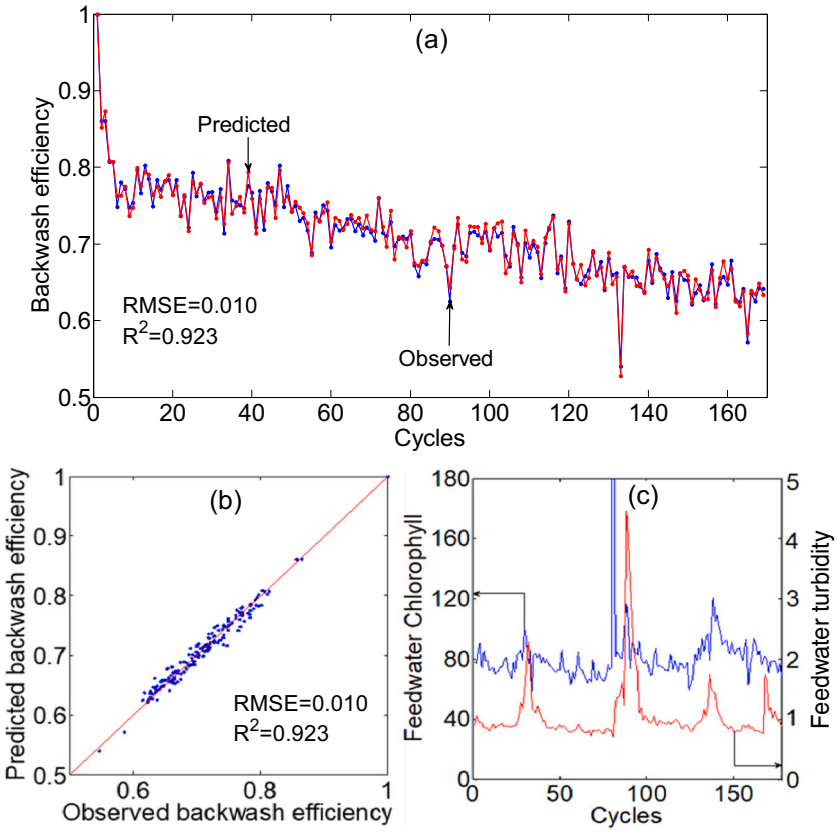

Fig. 10. Example of backwash efficiency predictions for dataset #TE22 in which the coagulant dose was constant (2.7 mg/L Fe^{3+}) and the raw seawater UF feed turbidity and *Chlorophyll a* exhibited the widest ranges of 0.6–4.4 NTU and 58–243.3 μg/L respectively): (a) variation of backwash efficiency with UF operational cycles, (b) predicted versus observed backwash efficiency, and (c) variability of feedwater turbidity and *Chlorophyll a*. UF operation period was 4 days with a total of 170 UF operational cycles.

Below the critical coagulant threshold dose, as the coagulant dose increases so does the rate of foulant cake formation, and in turn the backwash efficiency increases [43]. The above behavior is illustrated for test dataset #TE15 in Fig. 11a (also, Fig. S3, Section S3 Supplementary Material) for UF operation over a period of 3 days (130 UF operational cycles) in which the coagulant dose was incrementally lowered and then raised over the course of the test. The coagulant dose range remained below the critical threshold coagulant dose for the present UF RO seawater feed pretreatment [43].

BPNN-AEA model predictions, using the full attribute set, tracked the backwash efficiency decline to 74% as the coagulant dose was incrementally lowered from its initial value of 3 mg/L to 2.6 mg/L. Once the coagulant dose was incrementally raised, the backwash efficiency correspondingly increased. Over the entire operational period for the above dataset, feedwater quality, as quantified by turbidity and by *Chlorophyl a* fluctuated (Fig. 11c) over the range of 1.5–3.2 NTU 61–124 μg/L, respectively. Nonetheless, model predictions of backwash efficiency were excellent with R^2 and RMSE of 0.942 and 0.0083, respectively (Fig. 11b). However, when *Chlorophyll a* and turbidity were excluded from the set of attributes, model performance declined to $R^2 \sim$ 0.932 and RMSE~0.015. It is noted that if only one of either *Chlorophyll a* or turbidity are excluded, model performance is somewhat greater with $R^2 \sim 0.935$, RMSE~0.011 and $R^2 \sim 0.939$, RMSE~0.010, respectively, but lower relative to predictions with the full set of attributes.

A particularly revealing test of the ensemble model in tracking UF performance during a storm event (#TE23) is illustrated in Fig. 12, and Fig. S4 (Section S3, Supplementary Material) for backwash efficiency, post-backwash UF resistance and evolution of UF resistance, respectively. During the storm event, water quality in terms of turbidity and *Chlorophyl a* varied significantly (Fig. 12c) by 1.5–19 NTU and 43–142 μg/L fold, respectively, over the course of 8 days. Prior to the storm event, the post-backwash UF resistance increased steadily (Fig. S4, Section S3 Supplementary Material) for operation at a coagulant dose of 3.6–4.4 mg/L Fe^{3+}. However, once the coagulant dose controller was activated (about 10 cycles after the start of the storm event), the coagulant dose progressively increased up to a level of 4.4 mg/L Fe^{3+} by cycle 245. The post-backwash UF resistance continued to rise (by up to 25% of its pre-storm level), but after 300 UF operational cycles the backwash efficiency began to increase reaching a maximum at the highest dose level during the storm.

It is stressed that backwash efficiency can be greater than 100% given that foulant layer not backwashed in previous cycles may be removed in subsequent cycles [17,43]. The ensemble model accurately predicted the evolution of backwash efficiency (Fig. 12a and b) and post-backwash resistance (Fig. S4, Section S3 Supplementary Material), during the storm event, at a performance level of R^2 and RMSE 0.92 and 0.012, and 0.94 and 0.042, respectively). It is noted that exclusion of both *Chlorophyll a* and turbidity as model attributes (indicative of feedwater quality) reduces the backwash efficiency model performance to R^2 and RMSE of 0.906 and 0.019, respectively. When only one of

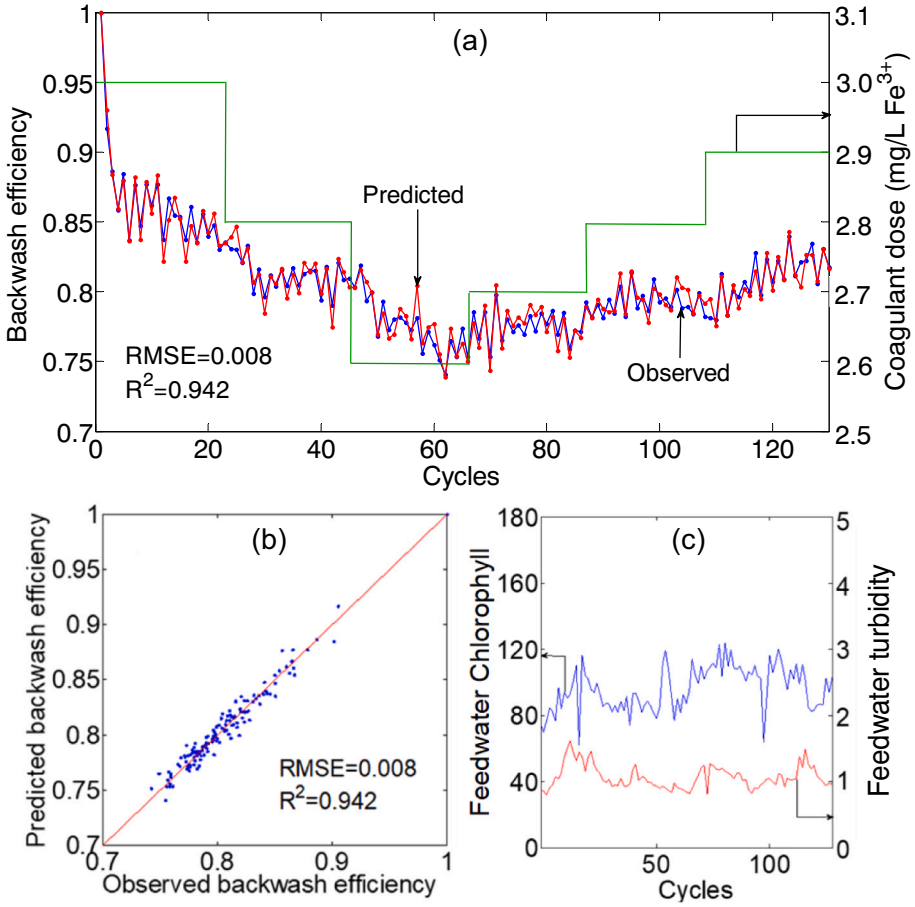

Fig. 11. Illustration of BPNN-AEA ensemble model predictions of UF backwash efficiency for operation with variable coagulant dose over 130 UF operational cycles of dataset #TE15 (3 days): (a) UF backwash efficiency predictions, (b) prediction versus field data of backwash efficiency, and (c) seawater UF feed turbidity and *Chlorophyll a* demonstrating variability in the ranges of 1.5–3.2 NTU and 61–124 μg/L, respectively.

either *Chlorophyll a* or turbidity were removed as input model attributes, model performance was further reduced to R^2 and RMSE of 0.916, 0.014 and 0.911, 0.017, respectively.

4. Conclusions

Ensemble BPNN model with AEA optimization was developed to describe the progression of ultrafiltration (UF) resistance during filtration and backwash in feed pre-treatment of RO seawater desalination. The model was developed based on an extensive 4-year operation of an integrated UF-RO seawater desalination system. The model demonstrated good predictive accuracy in describing UF time-series data which displayed temporal variability of UF performance in response to varying UF feedwater quality. Based on dataset of 422 days of UF-RO operation (consisting of 13.4 million data samples), over a wide range of water quality and operational settings (e.g., coagulant dose strategy), an ensemble model was developed following the AdaBoost strategy. The ensemble model was evaluated using test datasets for different operating conditions including a storm event that presented highly variable water quality conditions in terms of *Chlorophyll a* and turbidity. The ensemble model provided accurate predictive representation of UF operation in terms of UF membrane resistance during filtration and backwash, and of backwash efficiency and post-backwash UF resistance. In particular, the model described UF performance under dynamic conditions of variable coagulant dosing strategy. The excellent level of model performance suggests that there is potential for practical applications of the present machine-learning modeling approach to: (a) assess UF system performance drift such as deviation from expected baseline performance, (b) utilization of the approach for forecasting system performance based on expected changes in water quality, and (c) as a basis for model-based control of UF coagulant dosing control.

CRediT authorship contribution statement

Yang Zhou: Data analysis, model development, Writing – draft preparation. **Bilal Khan**: Workflow development and model review, Writing: draft preparation and review **Han Gu**: Field study, data compilation and UF performance analysis. **Panagiotis Christofides**: co-supervision of system development and UF performance analysis. **Yoram Cohen**: Study conceptualization, project supervision, modeling workflow review, Writing: draft preparation and review.

Declaration of competing interest

The authors declare that they have no known competing financial interests or personal relationships that could have appeared to influence the work reported in this paper.

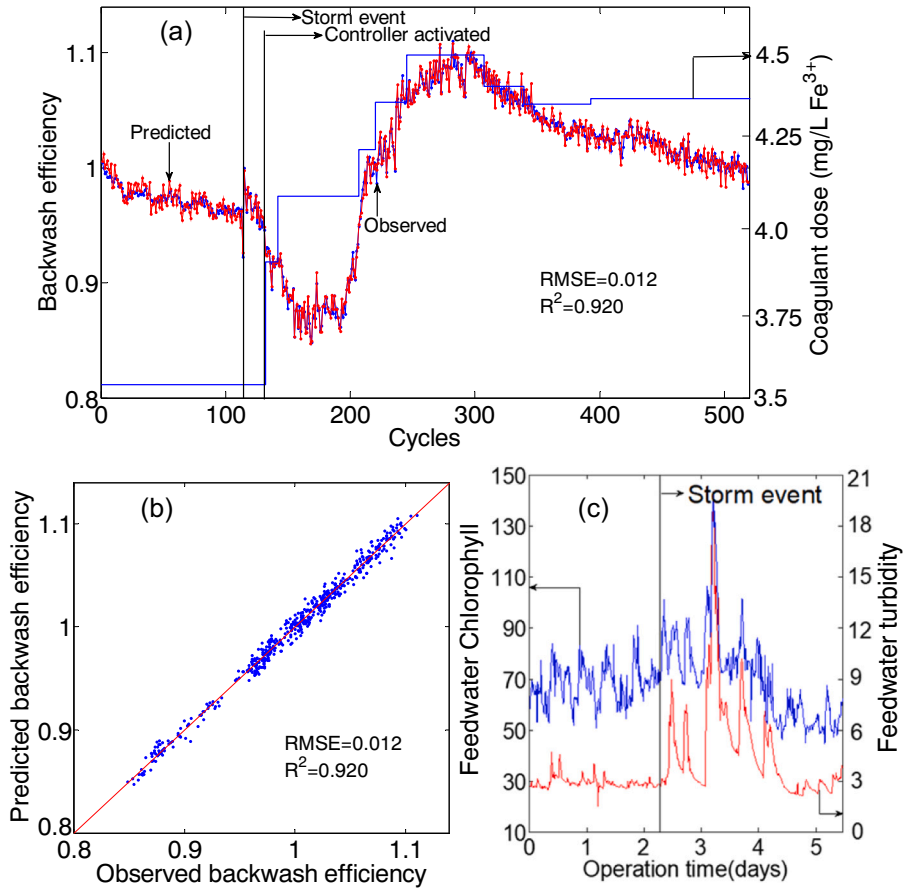

Fig. 12. Illustration of (a) UF backwash efficiency predictions on storm period (#TE23), (b) prediction versus field data, (c) Temperature, *Chlorophyll a* and turbidity (Note: turbidity, and *Chlorophyll a* were in the range of [1.5–19] NTU and [43 - 142] μg/L, respectively, during the above operational period), demonstrating the dependence of backwash efficiency on coagulant dose. R^2 and RMSE for the predictions are 0.920 and 0.0120, respectively.

Acknowledgements

This work was funded, in part, by the United States Office of Naval Research (N00014-11-1-0950 ONR and ONR N00014-09-1-1132), California Department of Water Resources (46-4120 and RD-2006-09), U.S. Bureau of Reclamation (R13AC80025), Naval Facilities Engineering Command (N62583-11-C-0630), the Grundfos Pumps Coporation, DuPont-Inge GmbH, and UCLA Water Technology Research (WaTeR) Center. The authors also acknowledge the technical assistance during the field study by personnel of the Naval Facilities Engineering and Expeditionary Warfare Center (NAVFAC EXWC) at Port Hueneme, CA, William Varnava, Mark Miller, Paul Giuffrida, Theresa Hoffard, Joseph Saenz, and Micah Ing.

Appendix A. Supplementary Material and Data

Detailed UF performance data can be found online at: doi:https://doi.org/10.5068/D1310B Supplementary material to this article can be found online at doi:https://doi.org/10.1016/j.desal.2021.115129.

References

[1] M. Elimelech, W.A. Phillip, The future of seawater desalination: energy, technology, and the environment, Science 333 (2011) 712–717.
[2] H. Carrao, G. Naumann, P. Barbosa, Mapping global patterns of drought risk: an empirical framework based on sub-national estimates of hazard, exposure and vulnerability, in: Global Environmental Change-Human And Policy Dimensions 39, 2016, pp. 108–124.
[3] L. Henthome, B. Boysen, State-of-the-art of reverse osmosis desalination pretreatment, Desalination 356 (2015) 129–139.
[4] L.O. Villacorte, S.A.A. Tabatabai, D.M. Anderson, G.L. Amy, J.C. Schippers, M. D. Kennedy, Seawater reverse osmosis desalination and (harmful) algal blooms, Desalination 360 (2015) 61–80.
[5] K.T. Chua, M.N.A. Hawlader, A. Malek, Pretreatment of seawater: results of pilot trials in Singapore, Desalination 159 (2003) 225–243.
[6] B. Ghernaout, D. Ghernaout, A. Saiba, Algae and cyanotoxins removal by coagulation/flocculation: a review, Desalin. Water Treat. 20 (2010) 133–143.
[7] R. Schurer, A. Tabatabai, L. Villacorte, J.C. Schippers, M.D. Kennedy, Three years operational experience with ultrafiltration as SWRO pre-treatment during algal bloom, Desalin. Water Treat. 51 (2013) 1034–1042.
[8] R. Schurer, A. Janssen, L. Villacorte, M. Kennedy, Performance of ultrafiltration and coagulation in an UF-RO seawater desalination demonstration plant, Desalin. Water Treat. 42 (2012) 57–64.
[9] C.Y. Tang, T.H. Chong, A.G. Fane, Colloidal interactions and fouling of NF and RO membranes: a review, Adv. Colloid Interf. Sci. 164 (2011) 126–143.
[10] M. Wilf, M.K. Schierach, Improved performance and cost reduction of RO seawater systems using UF pretreatment, Desalination 135 (2001) 61–68.
[11] A. Brehant, V. Bonnelye, M. Perez, Comparison of MF/UF pretreatment with conventional filtration prior to RO membranes for surface seawater desalination, Desalination 144 (2002) 353–360.
[12] K. Burashid, A.R. Hussain, Seawater RO plant operation and maintenance experience: Addur desalination plant operation assessment, Desalination 165 (2004) 11–22.
[13] O. Lorain, B. Hersant, F. Persin, A. Grasmick, N. Brunard, J.M. Espenan, Ultrafiltration membrane pre-treatment benefits for reverse osmosis process in seawater desalting. Quantification in terms of capital investment cost and operating cost reduction, Desalination 203 (2007) 277–285.
[14] P.H. Wolf, S. Siverns, S. Monti, UF membranes for RO desalination pretreatment, Desalination 182 (2005) 293–300.
[15] L.X. Gao, A. Rahardianto, H. Gu, P.D. Christofides, Y. Cohen, Novel design and operational control of integrated ultrafiltration - reverse osmosis system with RO concentrate backwash, Desalination 382 (2016) 43–52.
[16] H. Gu, A. Rahardianto, L.X. Gao, P.D. Christofides, Y. Cohen, Ultrafiltration with self-generated RO concentrate pulse backwash in a novel integrated seawater desalination UF-RO system, J. Membr. Sci. 520 (2016) 111–119.
[17] L.X. Gao, H. Gu, A. Rahardianto, P.D. Christofides, Y. Cohen, Self-adaptive cycle-to-cycle control of in-line coagulant dosing in ultrafiltration for pre-treatment of reverse osmosis feed water, Desalination 401 (2017) 22–31.

[18] S. Delgado Diaz, L. Vera Pena, E. Gonzalez Cabrera, M. Martinez Soto, L.M. Vera Cabezas, L.R. Bravo Sanchez, Effect of previous coagulation in direct ultrafiltration of primary settled municipal wastewater, Desalination 304 (2012) 41–48.
[19] E. Friedler, I. Katz, C.G. Dosoretz, Chlorination and coagulation as pretreatments for greywater desalination, Desalination 222 (2008) 38–49.
[20] K. Kimura, K. Tanaka, Y. Watanabe, Microfiltration of different surface waters with/without coagulation: clear correlations between membrane fouling and hydrophilic biopolymers, Water Res. 49 (2014) 434–443.
[21] S.A.A. Tabatabai, J.C. Schippers, M.D. Kennedy, Effect of coagulation on fouling potential and removal of algal organic matter in ultrafiltration pretreatment to seawater reverse osmosis, Water Res. 59 (2014) 283–294.
[22] J. Wang, J. Guan, S.R. Santiwong, T.D. Waite, Characterization of floc size and structure under different monomer and polymer coagulants on microfiltration membrane fouling, J. Membr. Sci. 321 (2008) 132–138.
[23] N. Porcelli, S. Judd, Chemical cleaning of potable water membranes: a review, Sep. Purif. Technol. 71 (2010) 137–143.
[24] Y.C. Woo, J.J. Lee, L.D. Tijing, H.K. Shon, M. Yao, H.-S. Kim, Characteristics of membrane fouling by consecutive chemical cleaning in pressurized ultrafiltration as pre-treatment of seawater desalination, Desalination 369 (2015) 51–61.
[25] C. Regula, E. Carretier, Y. Wyart, G. Gesan-Guiziou, A. Vincent, D. Boudot, P. Moulin, Chemical cleaning/disinfection and ageing of organic UF membranes: a review, Water Res. 56 (2014) 325–365.
[26] X. Shi, G. Tal, N.P. Hankins, V. Gitis, Fouling and cleaning of ultrafiltration membranes: a review, J. Water Process Eng. 1 (2014) 121–138.
[27] N.G. Cogan, J. Li, A.R. Badireddy, S. Chellam, Optimal backwashing in dead-end bacterial microfiltration with irreversible attachment mediated by extracellular polymeric substances production, J. Membr. Sci. 520 (2016) 337–344.
[28] A. Lok, H. Wray, P. Berube, R.C. Andrews, Optimization of Air Sparging and in-Line Coagulation for Ultrafiltration Fouling Control 188, Separation And Purification Technology, 2017, pp. 60–66.
[29] H. Chang, B. Liu, P. Yang, Q. Wang, K. Li, G. Li, H. Liang, Salt backwashing of organic-fouled ultrafiltration membranes: effects of feed water properties and hydrodynamic conditions, J. Water Process Eng. 30 (2019).
[30] E. Akhondi, F. Zamani, A.W.K. Law, W.B. Krantz, A.G. Fane, J.W. Chew, Influence of backwashing on the pore size of hollow fiber ultrafiltration membranes, J. Membr. Sci. 521 (2017) 33–42.
[31] Y. He, J. Sharma, R. Bogati, B.Q. Liao, C. Goodwin, K. Marshall, Impacts of aging and chemical cleaning on the properties and performance of ultrafiltration membranes in potable water treatment, Sep. Sci. Technol. 49 (2014) 1317–1325.
[32] S.A.A. Tabatabai, M.D. Kennedy, G.L. Amy, J.C. Schippers, Optimizing inline coagulation to reduce chemical consumption in MF/UF systems, Desalin. Water Treat. 6 (2009) 94–101.
[33] S. Jeong, F. Nateghi, N. Tien Vinh, S. Vigneswaran, T. Tuan Anh, Pretreatment for seawater desalination by flocculation: performance of modified poly ferric silicate (PFSi-delta) and ferric chloride as flocculants, Desalination 283 (2011) 106–110.
[34] A.H. Nguyen, J.E. Tobiason, K.J. Howe, Fouling indices for low pressure hollow fiber membrane performance assessment, Water Res. 45 (2011) 2627–2637.
[35] L. Gao, A. Rahardianto, H. Gu, P.D. Christofides, Y. Cohen, Energy-optimal control of RO desalination, Ind. Eng. Chem. Res. 53 (2014) 7409–7420.
[36] E. Zondervan, B. Blankert, B.H.L. Betlem, B. Roffel, Development of a multi-objective coagulation system for long-term fouling control in dead-end ultrafiltration, J. Membr. Sci. 325 (2008) 823–830.
[37] Y. Zhou, S. Li, BP neural network modeling with sensitivity analysis on monotonicity based Spearman coefficient, Chemom. Intell. Lab. Syst. 200 (2020), 103977.
[38] F. Yuan, J. Guo, Z. Xiao, B. Zeng, W. Zhu, S. Huang, A transformer fault diagnosis model based on chemical reaction optimization and twin support vector machine, Energies 12 (2019).
[39] Y. Zhou, S. Li, N. Xiong, Improved vine copula-based dependence description for multivariate process monitoring based on ensemble learning, Ind. Eng. Chem. Res. 58 (2019) 3782–3796.
[40] D. Gille, W. Czolkoss, Ultrafiltration with multi-bore membranes as seawater pre-treatment, Desalination 182 (2005) 301–307.
[41] Y. Cohen, P.D. Christofides, A. Rahardianto, A.R. Bartman, A. Zhu, H. Gu, L.X. Gao, Apparatus, System and Method for Integrated Filtration and Reverse Osmosis Desalination, U.S. Patent US9790113B2, in, USA, 2017.
[42] J.W. Chew, J. Kilduff, G. Belfort, The behavior of suspensions and macromolecular solutions in crossflow microfiltration: an update, J. Membr. Sci. 601 (2020).
[43] H. Gu, A. Rahardianto, L.X. Gao, X. Pascual Caro, J. Giralt, R. Rallo, P. D. Christofides, Y. Cohen, Fouling indicators for field monitoring the effectiveness of operational strategies of ultrafiltration as pretreatment for seawater desalination, Desalination 431 (2018) 86–99.
[44] J.D. Lee, S.H. Lee, M.H. Jo, P.K. Park, C.H. Lee, J.W. Kwak, Effect of coagulation conditions on membrane filtration characteristics in coagulation-microfiltration process for water treatment, Environ. Sci. Technol. 34 (2000) 3780–3788.
[45] Z. Li, H. Yan, C. Zhang, F. Tsung, Long-short term spatiotemporal tensor prediction for passenger flow profile, IEEE J. Robot. Autom. Lett. 5 (2020) 5010–5017.
[46] W. Chen, S. Wang, A 2nd-order ADI finite difference method for a 2D fractional black-Scholes equation governing European two asset option pricing, Math. Comput. Simul. 171 (2020) 279–293.
[47] J. Zhang, R. Agustriyanto, Multivariable inferential feed-forward control, Ind. Eng. Chem. Res. 42 (2003) 4186–4197.
[48] J. Kajornrit, P. Chaipornkaew, A comparative study of ensemble back-propagation neural network for the regression problems, in: J.L. Mitrpanont, W. Sawangphol (Eds.), 2017 2nd International Conference on Information Technology, 2017, pp. 55–60.
[49] H. Zhang, D. Yue, X. Xie, C. Dou, F. Sun, Gradient decent based multi-objective cultural differential evolution for short-term hydrothermal optimal scheduling of economic emission with integrating wind power and photovoltaic power, Energy 122 (2017) 748–766.
[50] S. Li, F. Li, Alopex-based evolutionary algorithm and its application to reaction kinetic parameter estimation, Comput. Ind. Eng. 60 (2011) 341–348.
[51] Y. Yang, X. Cheng, J. Cheng, D. Jiang, S. Li, Improved Alopex-based evolutionary algorithm by Gaussian copula estimation of distribution algorithm and its application to the Butterworth filter design, Int. J. Syst. Sci. 49 (2018) 160–178.